2013

Phase Composition Control of Calcium Phosphate Nanoparticles for Tunable Drug Delivery Kinetics and Treatment of Osteomyelitis. Part 1: Preparation and Drug Release

Vuk Uskoković
Chapman University, uskokovi@chapman.edu

Tejal A. Dasai
University of California - San Francisco

Recommended Citation

Uskoković V, Desai TA. Phase composition control of calcium phosphate nanoparticles for tunable drug delivery kinetics and treatment of osteomyelitis. Part 1: Preparation and drug release. *J Biomed Mater Res Part A*. 2013;101(5):1416-1426. doi:10.1002/jbm.a.34426.

Phase Composition Control of Calcium Phosphate Nanoparticles for Tunable Drug Delivery Kinetics and Treatment of Osteomyelitis. Part 1: Preparation and Drug Release

Published in final edited form as:
J Biomed Mater Res A. 2013 May ; 101(5): 1416–1426. doi:10.1002/jbm.a.34426.

Phase Composition Control of Calcium Phosphate Nanoparticles for Tunable Drug Delivery Kinetics and Treatment of Osteomyelitis. Part 1: Preparation and Drug Release

Vuk Uskoković and **Tejal A. Desai**
Therapeutic Micro and Nanotechnology Laboratory, Department of Bioengineering and Therapeutic Sciences, University of California, San Francisco

Abstract

Developed in this study is a multifunctional material for simultaneous osseoinduction and drug delivery, potentially applicable in the treatment of osteomyelitis. It is composed of agglomerates of nanoparticles of calcium phosphate (CAP) with different monophasic contents. The drug loading capacity and the release kinetics were investigated on two model drug compounds with different chemical structures, sizes and adsorption propensities: bovine serum albumin and fluorescein. Loading of CAP powders with small molecule drugs was achieved by physisorption and desiccation-induced agglomeration of nanoparticulate subunits into microscopic blocks. The material dissolution rate and the drug release rate depended on the nature of the CAP phase, decreasing from monocalcium phosphate to monetite to amorphous CAP and calcium pyrophosphate to hydroxyapatite. The sustained release of the two model drugs was shown to be directly relatable to the degradation rate of CAP carriers. It was demonstrated that the degradation rate of the carrier and the drug release kinetics could be made tunable within the time scale of 1–2 h for the most soluble CAP phase, monocalcium phosphate, to 1–2 years for the least soluble one, hydroxyapatite. From the standpoint of antibiotic therapy for osteomyelitis, typically lasting for six weeks, the most prospective CAP powder was amorphous CAP with its release time scale for a small organic molecule, the same category to which antibiotics belong, of 1 – 2 months under the conditions applied in our experiments. By combining these different CAP phases in various proportions, drug release profiles could be tailored to the therapeutic occasion.

Introduction

Nanomedical approaches are based on finely tuned and localized therapies that overcome many of the undesired side effects resulting from nonlocal distribution of therapeutic agents in the body.[1] Procedures for the synthesis of nanoparticles of practically every known composition have been developed over the past few decades[2], and the challenge ahead of us currently lies in preparation of multifunctional composite nanoparticulate systems.[3] The approach pursued in this study is based on the hypothesis that the development of a multifunctional nanoparticulate system that could simultaneously foster remineralization of the portion of bone lost to disease and release antibiotics at a finely tunable rate would improve the treatment of osteomyelitis.

Osteomyelitis, that is, bone infection caused by a variety of pathogens[4], many of which reside in healthy oral flora, affects mainly elderly and children and has been conventionally treated by means of (a) long-term antibiotic therapies[5], and (b) surgical removal of the portion of necrotic bony tissue[6]. While systemic distribution of the therapeutics in the body results from the former approach, the latter typically requires the application of extraneous implants to maintain the skeletal integrity of the affected area and/or minimize the effects of its unaesthetic disfigurement. Clear incentives thus exist for the development of more

advanced therapies based on (a) local and sustained delivery of antibiotics, and (b) osteogenic drug carriers.

Calcium phosphates (CAPs) have been traditionally considered as a suitable choice for the synthetic substitute of hard tissues due to their excellent biocompatibility, lack of cytotoxicity, non-immunogenicity, non-onconogenicity as well as sufficient loading capacities[7]. Hydroxyapatite (HAP), a CAP phase naturally present in hard tissues, is the most stable one under physiological conditions; however, the downside of this exceptional chemical stability and sufficient compressive strength of HAP is its rather slow resorption kinetics[8]. The second most commonly used CAP phase is tricalcium phosphate (TCP); however, its degradation rate is thought to be too high to match the new bone growth rate[9]. Optimization of the phase composition of CAP used for bone grafting purposes has consequently grown into a conventional approach to improving the biodegradability of CAP-based biomaterials while preserving their strength during the past three decades[10,11]. Most of these materials have, however, been composed of mainly two phases: HAP and TCP[12]. Yet, as can be seen from Table 1, solubility of CAPs can be optimized within a wide range of values, from highly soluble monocalcium phosphates (pK_{sp} = 1.14) to sparsely soluble HAP (pK_{sp} = 117.3). In this work, we have focused on assessing solubility behavior, along with the drug release profiles, of a few rarely used CAP phases, including HAP. Starting from the assumption that the drug release rate can be made directly proportional to the degradation rate of the particles encapsulating the drug, optimization of the latter by means of controlling the stochiometry of the drug delivery carrier has been the approach followed in this study.

Experimental part

Synthesis of CAP powders

CAP powders with various monophase compositions were prepared by direct precipitation from aqueous solutions, as described by the following reaction:

$$Ca^{2+}_{(aq)} + H_xPO_4^{x-3}{}_{(aq)} + H_3O^+/OH^- \leftrightarrow CAP_{(s)} \quad \text{(Eq.1)}$$

(Eq.1)

The method for preparation of HAP was adapted and modified from Ref.[17]. It began with adding 400 ml of 0.06 M aqueous solution of $NH_4H_2PO_4$ containing 25 ml 28 % NH_4OH dropwise (13.333 ml/min) to the same volume of 0.1 M aqueous solution of $Ca(NO_3)_2$ containing 50 ml 28 % NH_4OH, vigorously stirred with a magnetic bar (400 rpm) and kept on a plate heated to 50 °C. After the addition of $NH_4H_2PO_4$ was complete, the suspension was brought to boiling, then immediately removed from the heater and let cool in air. Stirring was suspended and the precipitate alongside its parent solution was left to age in atmospheric conditions for 24 h. After the given time, the precipitate was washed once with deionized (DI) H_2O, centrifuged (10 sec at 3500 rpm), and let dry overnight in a vacuum oven (p = − 20 mmHg) at 80 °C.

To synthesize monetite (dicalcium phosphate anhydrous; DCPA, $CaHPO_4$), the same procedure was repeated using 400 ml 0.33 M $Ca(NO_3)_2$ and 400 ml 0.25 M $NH_4H_2PO_4$ containing 10 ml 28 % NH_4OH, with bringing the suspension to boiling afterwards. To synthesize calcium pyrophosphate (CPP, β-$Ca_2P_2O_7$), the same procedure was repeated using the same volumes of 0.2 M $Ca(NO_3)_2$ containing 3 ml of 28 % NH_4OH and 0.25 M $NH_4H_2PO_4$ supplemented with 28 % NH_4OH until pH 6.8 was reached. Following precipitation and drying, the loose powder was annealed in a *Barnstead Thermolyne 1300* furnace at 800 °C for 2 h, with the heating and cooling rates of 10 °C/min.

The synthesis of monocalcium phosphate monohydrate ($Ca(H_2PO_4)_2{\cdot}H_2O$, MCPM) was carried out by mixing identical volumes of 3.5 M H_3PO_4 (40 wt% conc. H_3PO_4) and 1.8 M $Ca(NO_3)_2$. The transparent mixture was intensively agitated using a magnetic bar and brought to boiling. When approximately two-thirds of the liquid evaporated, the precipitation occurred and a white suspension was formed. Stirring was immediately discontinued, lest DCPA formed due to extensive evaporation. The sol was let cool down and turn into a gel at room temperature. To prevent precipitation at a very high supersaturation when the precipitate solidifies and becomes virtually unsuspendable, the temperature of the heating plate did not exceed 250 °C. The gel was repeatedly alternately centrifuged and washed with ethanol to remove H_3PO_4, separated from the supernatant, dried for 30 min at room temperature and stored at 4 °C to prevent transformation to DCPA.

Amorphous CAP (ACP) was formed by abruptly adding a solution containing 100 ml 0.5 M $Ca(NO_3)_2$ and 7 ml 28 % NH_4OH into a solution comprising 100 ml 0.2 M $NH_4H_2PO_4$ and 4 ml 28 % NH_4OH. The fine precipitate formed upon mixing was aged for 15 s, before it was collected, centrifuged, washed with 0.14 w/v% NH_4OH, centrifuged again, dried overnight at low pressure (p = − 20 mmHg) and room temperature, and stored at 4 °C to prevent spontaneous transformation to HAP. Table 2 lists ionic concentrations and pHs of $Ca(NO_3)_2$ and $NH_4H_2PO_4$ solutions prior to their mixing, along with the final pH of the solution in equilibrium with the precipitate and the crystallite size of such obtained powders.

CAP solubility experiments

Solubility of synthesized CAP powders was evaluated in a twofold manner. First, 10 mg of each CAP powder, except MCPM, were placed in separate 10 ml of either 20 mM Tris/HCl (pH 7.4) or 20 mM MES/NaCl (pH 6.0) and incubated at room temperature. For MCPM, 10 times higher concentration of the buffers was used to prevent pH drop due to a considerable release of free protons and $HPO_4^{2-}/H_2PO_4^-$ ions upon its dissolution. The concentration of free calcium ions in the solution ($[Ca^{2+}]$) was read periodically using Ca^{2+} microelectrode in combination with a reference electrode (*Microelectrodes, Inc.*) on an Accumet AR15 pH-meter (*Fisher Scientific*). The solution was replaced every 24 h to prevent saturation and minimize the effects of spontaneous re-precipitation. The average dissolution rate was calculated as:

$$\Sigma_{1\rightarrow n}([Ca]_{t2} - [Ca]_{t1})/n(t_2 - t_1)[Ca^{2+}]_{total} \quad \text{(Eq. 2)}$$

(Eq. 2)

$[Ca]_{t2}$ and $[Ca]_{t1}$ represent two measured concentrations of free Ca^{2+} ions at two successive time points; n is the number of data points; t_2 and t_1 stand for two successive time points; and $[Ca^{2+}]_{total}$ equals the total concentration of free Ca^{2+} ions upon complete dissolution of the powder. The second dissolution test involved placing 10 mg of each CAP powder, except MCPM, in separate 10 ml of 20 mM Tris/HCl (pH 7.4) solution and incubation at room temperature. As in the first dissolution test, MCPM was immersed in 200 mM Tris/HCl (pH 7.4). The acidic solution of 2 M HCl was added in increments of 1 – 10 μl to gradually lower the pH. After 5 min of incubation at each pH, $[Ca^{2+}]$ was read using Ca^{2+} microelectrode in combination with a reference electrode. The degree of saturation (DS) was calculated using an algorithm based on Debye-Hückel equation[18].

Drug loading and release

To test the drug loading efficiency and release kinetics, CAP particles with different phase compositions were loaded by physisorption with a moderately sized polypeptide, fluorescein-isothiocyanate-tagged bovine serum albumin (FITC-BSA; 66.5 kDa; 14 × 4 × 4

nm^3, *Sigma*), and a small organic molecule, fluorescein sodium ($C_{20}H_{10}Na_2O_5$; logP = 3.4; M_w = 376.28 g/mol, d ~ 0.7 nm, *Fluka*). The latter compound was chosen due to its similarity in size and hydrophilicity to clindamycin ($C_{18}H_{33}ClN_2O_5S$; logP = 1.6; M_w = 424 g/mol), the antibiotic loaded in the later stages of the study. More details about the loading procedure are given in the supplementary section. Drug release experiments were conducted by immersing 10 mg of each CAP powder separately in 1 ml of 20 mM Tris/HCl (pH 7.4) and incubating them at room temperature for up to 10 days. A portion of the solution (100 μl) was sampled out periodically and analyzed for fluorescence convertible to concentration. The medium was replaced every 24 h to prevent saturation and minimize spontaneous re-precipitation. At the end of the 200 h release time, the remaining powders were dissolved in 20 mM HCl. The resulting fluorescence was measured and used to calculate the overall amount of the drug initially contained by the powders. The dissolution and the consequential drug release amounts settled under these measurement conditions already after 24 – 48 h, allowing for extrapolation of the given values from the known average daily amounts of the dissolved powder or a released drug and eliminated the necessity for long-term measurements.

Structural and morphological characterization

X-ray diffraction (XRD) studies were carried out on a *Siemens* D500 diffractometer using $Cu_{K\alpha}$ = 1.5418 Å as the wavelength of the radiation source. The average size of the crystallites was determined using a structural refinement approach (Topas 2.0) based on the previously identified crystal structure (PCPDFWIN & Eva). The step size was 0.04 °, with 1 s of sample irradiation time per step. The morphology of the powders was analyzed on a *Hitachi* S-4300SE/N scanning electron microscope (SEM) equipped with an energy dispersive X-Ray (EDX) analyzer at the electron beam energy of 15 kV. Zeta-potential values in the pH range of 4 – 10 were measured in water using a *Malvern* Zetasizer Nano Series.

Results and Discussion

Literature reports on using CAPs as drug delivery carriers have been steadily increasing over years.[19–23] On the other hand, studies aimed at developing CAP particles for tunable drug release have been far less numerous.[24–26] Moreover, most of them focused on release of proteins, compounds that much more efficiently adsorb onto mineral surface than small organics, the category into which antibiotics fall. In this work, we decided to focus on five different monophasic compositions of CAPs, covering their entire range of solubility products, from pK_{sp} 1 to 117 (Fig.1a). XRD patterns of the prepared monophasic CAP powders are shown in Fig.1b. Some phases were omitted: OCP due to (a) the proximity of its K_{sp} to that of HAP (Table 1) and (b) the fact that it is a metastable polymorph that tends to spontaneously transform to HAP with an increase of the reaction temperature or time[27,28]; TCP owing to (a) the fact that calcination, during which sintering of grains often occurs[29], is required for its formation, and (b) the proximity of its K_{sp} to K_{sp} reported for various forms of ACP obtained under similarly alkaline conditions of precipitation as those used in this study (Table 1).

Ideally, a single synthesis parameter would be varied for the sake of controlling the phase composition of precipitated CAP powders and tuning their solubility over a wide range of values. However, this approach did not prove to be viable in reality, as in accordance with the need to apply different methods of precipitation to obtain different CAP phases outlined by Hodge *et al.* in 1938: “The composition of the precipitated phosphates is seen to depend upon the mode of precipitation rather than the amount of reactants”[30]. Correspondingly, a variation of pH in the method used to precipitate HAP was shown to yield only DCPA at pH < 6 when precipitation was carried out at 50 °C (Fig.2a) and at pH ≤ 5 when CAP sol was

brought to boiling following its precipitation (Fig.2b). Also, a simple variation of Ca/P molar ratio, which increases in more or less direct proportion with pK_{sp} (Table 1), yielded HAP powders with identical XRD patterns and unmodified crystallite sizes (12 nm) and morphologies. Variations in the rate of addition of the precursor $NH_4H_2PO_4$ solution to $Ca(NO_3)_2$ were earlier shown to affect only the stoichiometry of the resulting CAP powders, but not their phase composition.[31] Different methods thus had to be used to obtain different CAP phases: precipitation from solutions with low degrees of saturation and high Ca/P ratios was applied in the synthesis of HAP and DCPA; abrupt mixing of reactants that produced conditions of ultrahigh supersaturation and nucleation rate was used to prepare ACP; evaporation of solutions at low pH and low Ca/P ratios was used in the formation of MCPM; annealing of a precipitated mixture of DCPA and HAP at a moderately high temperature was applied to yield CPP.

The size of HAP and DCPA crystallites corresponding to XRD patterns in Fig.2 was in the nano range: 30 – 60 nm for DCPA and 5 – 17 nm for HAP synthesized directly, without bringing the colloidal suspension to boiling, and 50 – 90 nm for DCPA and 3 – 12 nm for HAP whose preparation was coupled to the boiling step. In general, whereas boiling promoted an increase in the crystallite size for DCPA, it had an opposite effect for HAP. In the case of DCPA, boiling was shown to be necessary to prevent coalescence of the particles and retain the nanoparticulate nature of the precipitate. The monodisperse and nanosized nature of DCPA powder prepared using boiling (Fig.3a) differs from smooth microsized plates formed when the boiling step is omitted (Fig.3b). Since precipitation of CAP is an endothermal process[32,33], an increase in temperature will, according to Le Châtelier's principle, yield lower solubility and greater supersaturation. Consequently, boiling leads to completion of the solidification process and prevents the ripening effect and formation of layered structures, such as those displayed in Fig.3b. The final pH of the precipitation reaction had an effect on the crystallite size, but only in the case of as-precipitated powders (Fig.2a): the lower it was during the formation of DCPA, the greater the crystallinity of the powder, while the opposite trend was observed for HAP. In contrast, when boiling was applied following precipitation, there was no variation in the crystallinity of the powders depending on the pH (Fig.2b).

SEM images of HAP and other CAP powders are shown in Fig.3. The morphological analysis of CAP samples indicates their unequivocally spherical and nanosized character. The particle size was found in the range from 20 – 100 nm for the non-annealed phases, HAP, ACP, DCPA and MCPM, to 100 – 300 nm for the only annealed phase, CPP. In the case of MCPM, the nanoparticles exhibited a tendency to aggregate into plates of 1 – 3 μm in length and 100 – 200 nm in thickness (Fig.3e). To ensure that CPP powder retained the nanoparticulate nature of its precipitated precursor, annealing of comparatively low intensity was used for its formation: 800 °C for 2 h (Fig.S1). This phase was chosen over TCP, another CAP phase obtainable strictly through calcinations, because of its significantly higher proneness to bioresorption[34], upon which the drug release is expected to be directly contingent.

Results of the tests designed to assess the solubility of different CAP phases at two different pHs, the physiological (7.4) and the mildly acidic one (6.0), are shown in Fig.4. At both pHs, the highest solubility was expectedly exhibited by MCPM, as in 1–2 h the dissolution of the material reached completion. The dissolution process still took place not instantaneously, but gradually under static conditions of incubation applied in the tests. The second highest solubility was exhibited by DCPA, as it took approximately a week for it to completely dissolve at pH 7.4 and 2–3 weeks at pH 6.0. As in agreement with the stochiometric solubility data (Table 1), the solubility of ACP was lower than that of DCPA, but higher than that of HAP. If extrapolated along the time axis, it could be shown that

dissolution of ACP at pH 7.4 would be over in about 3 months, as opposed to a year in the case of HAP, all under the solubility measurement settings based on daily replacement of the solution and the given concentration of the solid phase (1 mg/ml). If extrapolation of values obtained only during the first hour of dissolution following medium replacement at pH 7.4 is carried out, the estimated time until total dissolution becomes lower for all phases except MCPM: 2 months for HAP, 1 week for ACP, and 10 h for DCPA. As dictated by the thermodynamic propensities of HAP, its solubility is greater at pH 6.0 than at pH 7.4, although negligibly, increasing from 0.25 to 0.3 % per day. Extrapolation of values obtained only during the first hour of dissolution following medium replacement at pH 6.0 again yields lower estimated times until total dissolution for all phases except MCPM: 2 months for HAP, 2 weeks for ACP, and 3 days for DCPA. Overall, the comparison of solubilities at two different pHs has yielded the following insights: MCPM has not shown significant difference in solubility behavior depending on the pH; alkaline ACP and HAP have expectedly demonstrated increased solubility at the lower pH; DCPA, owing to the presence of a proton in its stoichiometric formula and, consequently, a greater stability under mildly acidic conditions, has shown higher resistance to dissolution at pH 6.0 than at pH 7.4. Table 3 compiles the data on dissolution time scales and rates for four different CAP powders.

The dissolution of CPP was shown to exhibit the lowest initial burst in dissolved material (Fig.4c). The reason for this presumably lies in its much lesser content of amorphized and easily soluble material on the particle surface compared to as-precipitated powders. The initial dissolution rate was much higher for ACP and HAP, which is, conversely, most likely caused by the relatively disordered particle surface of as-precipitated solids, which entropically favors their dissolution in comparison with the more crystalline particle core. After only a few hours of dissolution, however, the dissolution rate of CPP stabilizes and maintains an identical value as that of ACP throughout the rest of the incubation time. Due to this identicality, CPP was exempted from the subsequent drug release studies. The dissolution rate for CPP at pH 7.4 was found to be 0.8 % per day, while time to its complete dissolution was equal to that of ACP, i.e., approximately 3 months, or about 2 weeks, double that of ACP, when the results were extrapolated for 1 h medium replacement. During the dissolution of HAP and ACP, the amount of the dissolved solid phase drastically drops down after a few initial sets of medium replacements (Fig.S3). This effect is consistent with the regularly observed incongruent, nonstochiometric dissolution of CAPs[35,36] whereby surface recrystallization of more stable phases under the given conditions hinders dissolution of the less stable underlying phase by shielding it from the undersaturated solution. This incongruent dissolution owing to which particles, effectively, act as buffers against their own dissolution is not necessarily an undesirable phenomenon since it prolongs the retention of the material in the target zone, while promoting the rapid initial degradation period and drug release through which the minimal concentration for inhibiting the bacterial growth is rapidly exceeded. Incongruency upon dissolution has also implied that even for samples equilibrated for 19 months, the solubility differed depending on the amount of solid phase added to a given volume of the solvent[37]. To minimize the effects of reprecipitation, the dissolution experiments were carried out by means of daily replacement of the solution media, as opposed to standard methods involving the usage of a constant solution throughout prolonged periods of time. Such solubility measurements can also be said to better mimic *in vivo* effects of dynamic circulation flow than the static ones.

The results of the second dissolution test that involved a gradual decrease in pH and relatively short equilibration periods are shown in Fig.4d. The same trend of dissolution capacity increase from HAP to ACP to DCPA to MCPM was confirmed during this test. During the dissolution of DCPA, at pH 6.2 and DS = 9 – 11, a re-precipitation event of thermodynamically the most stable CAP phase to precipitate under these conditions, HAP, was detected. Due to intrinsic alkalinity of HAP, crystallization of this barely stable new

phase lowers pH and speeds up its own dissolution; hence, at pH 4.6, [Ca^{2+}] reaches 5.8 mM, much higher than 4.4 mM at pH 6.6. The broad time scale of the degradation of CAP phases synthesized in this study, ranging from a few hours to a couple of months or longer, offers promises for designing the desirable drug release kinetic profiles by mixing these powders in different ratios.

Fig.3c has illustrated the transition that CAP nanoparticles underwent during desiccation: aggregation into compact microsized blocks. The naturally rough surface of CAP particles exhibits topographic irregularities on the atomic scale[38,39], which does not only favor protein adsorption[40], osteoblast differentiation[41] and expression of osteogenic markers[42], but also causes high levels of adhesion upon contact, promoting facile formation and retention of stable aggregates even under relatively intensive agitations in the solution. This propensity of the particles to form aggregates subsequently stable in solution was used as the primary mechanism for loading the powders with small organic molecules. Aside from the fact that aggregation can protect the adsorbed drug against degradation, it has also proven to be a vital means for sustaining the gradual release of the pharmaceutics when the material is brought into contact with aqueous solution.

Post-precipitation addition of adsorbate in the form of BSA, one of two model drug compounds used, was shown to yield greater loading efficiency than co-precipitation of CAP and the organic molecules (Fig.5). It is assumed that BSA sequesters free Ca^{2+} ions and inhibits the nucleation of HAP, as previously observed[43,44] and evidenced by visually delayed onset of precipitation during the dropwise addition of the $H_xPO_4^{x-3}$ solution as well as lesser turbidity of the resulting CAP sol with BSA present in the Ca^{2+} solution. The visible comparison of the two precipitates at the titration endpoint has thus shown a larger amount of particles formed when precipitation was performed in the absence of BSA. In contrast, BSA, utilized in biochemistry labs as a nonspecific binding agent, binds well to most surfaces. Once the particles are formed, its binding, owing to an already existing surface, thus proceeds much more effectively. In contrast, the loading efficiency for fluorescein was the same, regardless of whether the drug was added to solution before the precipitation of HAP or after it (Fig.5). Post-precipitation BSA adsorption efficiency for HAP was by almost two orders of magnitude higher than for fluorescein, which can be explained by the very high potential of HAP to bind proteins, the reason for which it has been used as an adsorbent of peptides and nucleic acids in chromatographic columns[45,46]. Co-precipitation adsorption efficiency was, on the other hand, almost equal for BSA and fluorescein on HAP. Since Ca^{2+} ions present primary binding ions on CAP surface, BSA, comprising Ca^{2+}-binding amino acid residues along its sequence[47], tends to be attracted to it more specifically than fluorescein. The difference between ζ-potentials of HAP and BSA is, more or less, constant in the entire pH range of their mutual stability (4 – 10; Fig.6), which indicates that efficient electrostatically driven adsorption could occur independently of pH. As demonstrated earlier, owing to alternation of charged Ca^{2+} and PO_4^{3-} ions of CAP surface, the latter adsorbs both acidic and alkaline proteins, regardless of its actual ζ-potential and net charge.[48] Like BSA, fluorescein also exhibits negative charge at pH > 5 due to the presence of a carboxyl group ($pK_a \approx 5$) and a phenol group ($pK_a \approx 6.4$)[49], which favors its attraction to Ca^{2+} ions on CAP surface.

As could be seen from Fig.7a–b, the trend in the release rate of two model drug compounds encapsulated within CAP powders tends to be the same as the one observed for the dissolution rate of the given powders. The release of both drugs from MCPM thus reaches completion in 1–2 h; fluorescein release from DCPA is practically complete after a week and reaches 80 % after 10 days for BSA; the drug release from ACP reaches 70 % after 10 days for fluorescein and 50 % for BSA; the released amount of both drugs from HAP is approximately 30 – 40 % after 10 days. This indicates that the kinetics of the degradation of

the carrier greatly determines the temporal profile of the release of the drug. The amount of the released drug in percentages still exceeds that of the dissolved material, which coincides with the organic molecules being adsorbed on the surface of the particle rather than being encapsulated internally, in pores and crystalline crevices. The rate of release of fluorescein was higher at any time point and for all CAP phases than that of BSA, which can be explained by its lower adsorption intensity, inversely proportional to desorption propensity which kinetically precedes the release of the drug. Fluorescein release rate also exponentially decreases, while BSA release is more continuous, additionally speaking in favor of BSA being adsorbed more intensively and the release of fluorescein being caused by undersaturation effect to a greater extent. Fig.7c shows a drastic difference in time release profiles for fluorescein from dried and undried ACP powders and a negligible one for BSA. The release of fluorescein from undried ACP is markedly faster, which is due to the lack of formation of firm aggregates, a consequence of the omitted compaction of nanoparticles during their desiccation. In contrast, the release kinetics of BSA does not significantly change depending on whether it is released from dry and dense powders or undried and loose ones where nanoparticles retained their individual nature, indicating that the release of BSA is conditioned by the kinetics of its resorption from CAP surface, while sustained fluorescein release is contingent upon particle aggregation during drying.

The driving force for the dissolution of the powders and the release of the drug is naturally undersaturation of the liquid medium with respect to the ionic species that comprise the solid phase, while the reason for the decrease in the rate of release over time is presumably partly due to the amorphous and easily soluble content of the powder on the particle surface as well as to the drug molecules weakly adsorbed on it. Once the drug release becomes solely contributed to by the internally confined drug molecules, the release mechanism becomes governed by the complex relationship between the pore size in the material, its degradation rate, the size of the outwardly diffusing molecules and their binding energy, which is known to often result in zero-order kinetics.[50] Finally, from the standpoint of antibiotic therapy for osteomyelitis, typically lasting for six weeks[5], the most prospective CAP powder is ACP with its release time scale for a small organic molecule, the same category to which antibiotics belong, of 1 – 2 months under the conditions applied in our experiments.

Summary

The ongoing trend of increase in the number of infectious bone diseases, along with the imperfect state-of-the-art therapies, highlights the need for finding convenient new ways for their treatment. Steps towards developing a bioactive nanostructured material for simultaneous (a) controlled and sustained drug delivery and (b) remineralization of hard tissue lost to disease are presented in this report. In this work, the emphasis was on the synthesis of biocompatible and osteoconductive drug delivery carriers with tunable degradation and drug release kinetics. In the past and with respect to the broad spectrum of phase compositions of CAPs, only two CAP phases were utilized for the sake of controlling the biodegradation rate of monophasic or biphasic mixtures thereof: HAP and TCP. In particular, the approach to bone regeneration by means of surgical implantation of synthetic calcium phosphates has paradigmatically relied on HAP, the CAP phase already present in bone. In this study, we have focused on four different phases, alongside HAP, and a much broader range of solubilities, from $pK_{sp} = 1$ to $pK_{sp} = 117$. A set of monophasic CAP powders with solubilities and corresponding drug release time scales ranging from 1–2 h to 1–2 years was thus synthesized. The sustained release of two model drugs, BSA and fluorescein, was shown to be directly relatable to the degradation rate of CAP carriers. Efficient loading of BSA by physisorption and its sustained release were shown to be independent of the drying-induced aggregation of CAP nanoparticles into larger blocks,

which the prolonged release and loading of fluorescein was shown to be contingent upon. In theory, by combining these different CAP phases in various proportions, drug release profiles could be tailored to the therapeutic occasion. By varying the phase composition of the particles, an optimal balance between bioactivity and biodegradability could be achieved, so as to provide an osteoconductive surface for osteoblasts to adhere onto and match the rather slow rate of the formation of new bone, while at the same time ensuring sufficient degradation and drug release rates to eradicate the pathological source of infection and provide ionic species that will serve as ingredients of the newly forming bony tissues.

Supplementary Material

Refer to Web version on PubMed Central for supplementary material.

Acknowledgments

Presented were the results of a study supported by the NIH grant K99-DE021416.

References

1. Riehemann K, Schneider SW, Luger TA, Godin B, Ferrari M, Fuchs H. Nanomedicine-Challenge and Perspectives. Angew Chem Int Ed. 2009; 48:872–897.
2. Uskoković V, Drofenik M. Synthesis of Materials within Reverse Micelles. Surf Rev Let. 2005; 12:239–277.
3. Uskoković V, Uskoković DP. Nanosized hydroxyapatite and other calcium phosphates: Chemistry of formation and application as drug and gene delivery agents. J Biomed Mat Res B. 2011; 96B: 152–191.
4. Del Pozo JL, Patel R. Infection Associated with Prosthetic Joints. New Eng J Med. 2009; 361:787–794. [PubMed: 19692690]
5. Mouzopoulos G, Kanakaris NK, Kontakis G, Obakponovwe O, Townsend R, Giannoudis PV. Management of bone infections in adults. Injury. 2011; 42:S18–S23. [PubMed: 22196905]
6. Cunha BA. Osteomyelitis in Elderly Patients. Clin Inf Diseases. 2002; 35:287–293.
7. Kretlow JD, Young S, Klouda L, Wong M, Mikos AG. Injectable Biomaterials for Regenerating Complex Craniofacial Tissues. Adv Mat. 2009; 21:3368–3393.
8. Dorozhkin SV. Biphasic, triphasic and multiphasic calcium orthophosphates. Acta Bio. 2012; 8:963–977.
9. Guo D, Xu K, Han Y. The in situ synthesis of biphasic calcium phosphate scaffolds with controllable compositions, structures, and adjustable properties. J Biomed Mat Res A. 2009; 88A: 43–52.
10. Daculsi G, Legeros RZ, Nery E, Lynch K, Kerebel B. Transformation of biphasic calcium phosphate ceramics in vivo: ultrastructural and physicochemical characterization. J Bio Mat Res. 1989; 23:883–894.
11. Lukić M, Stojanović Z, Škapin SD, Maček-Kržmanc M, Mitrić M, Marković S, Uskoković D. Dense finegrained BCP bioceramics designed by two-step sintering. J Europ Ceram Soc. 2011; 31:19–27.
12. Kundu B, Soundrapandian C, Nandi SK, Mukherjee P, Dandapat N, Roy S, Datta BK, Mandal TK, Basu D, Bhattacharya RN. Systematic approach to treat chronic osteomyelitis through ceftriaxone–sulbactam impregnated porous β-tri calcium phosphate localized delivery system. Ceram Int. 2012; 38:1533–1548.
13. Dorozhkin SV. Calcium Orthophosphates in Nature, Biology and Medicine. Materials. 2009; 2:399–498.
14. Combes C, Rey C. Amorphous calcium phosphates. Acta Biomat. 2010; 6:3362–3378.
15. Magalhaes, MCF.; Marques, PAAP.; Correia, RN. Calcium and Magnesium Phosphates: Normal and Pathological Mineralization. In: Königsberger, Erich; Königsberger, LanChi, editors.

Biomineralization – Medical Aspects of Solubility. New York, NY: Wiley-Blackwell; 2007. p. 71-123.

16. Webb NC. The Crystal Structure of β-$Ca_2P_2O_7$. Acta Cryst. 1966; 21:942–948.
17. Marković S, Veselinović L, Lukić MJ, Karanović L, Bračko I, Ignjatović N, Uskoković D. Synthetical bone-like and biological hydroxyapatites. Biomed Mater. 2011; 6 045005.
18. Larsen, MJ. Ion Products and Solubility of Calcium Phosphates. Royal Dental College; 2001.
19. Tabaković A, Kester M, Adair JH. Calcium phosphate-based composite nanoparticles in bioimaging and therapeutic delivery applications. Wiley Interd Rev: Nanomed Nanobiotech. 2012; 4:96–112. (2012).
20. Epple M, Ganesan K, Heumann R, Klesing J, Kovtun A, Neumann S, Sokolova V. Application of calcium phosphate nanoparticles in biomedicine. J Mat Chem. 2010; 20:18–23.
21. Ginebra MP, Traykova T, Planell JA. Calcium phosphate cements as bone drug delivery systems: A review. J Contr Release. 2006; 113:102–110.
22. Bose S, Tarafder S. Calcium phosphate ceramic systems in growth factor and drug delivery for bone tissue engineering: A review. Acta Biomat. 2012; 8:1401–1421.
23. Verron E, Khairoun I, Guicheux J, Bouler JM. Calcium phosphate biomaterials as bone drug delivery systems: a review. Drug Discov Today. 2010; 15:547–552. [PubMed: 20546919]
24. Dasgupta S, Bandyopadhyay A, Bose S. Reverse micelle-mediated synthesis of calcium phosphate nanocarriers for controlled release of bovine serum albumin. Acta Biomat. 2009; 5:3112–3121.
25. Matsumoto T, Okazaki M, Inoue M, Yamaguchi S, Kusunose T, Toyonaga T, Hamada Y, Takahashi J. Hydroxyapatite particles as a controlled release carrier of protein. Biomaterials. 2004; 25:3807–3812. [PubMed: 15020156]
26. Lee JS, Suarez-Gonzalez D, Murphy WL. Mineral Coatings for Temporally Controlled Delivery of Multiple Proteins. Adv Mater. 2011; 23:4279–4284. [PubMed: 22039597]
27. Elliott, JC. Structure and Chemistry of the Apatites and Other Calcium Orthophosphates. Amsterdam, NL: Elsevier; 1994.
28. Arellano-Jiménez MJ, García-García R, Reyes-Gasga J. Synthesis and hydrolysis of octacalcium phosphate and its characterization by electron microscopy. J Phys Chem Solids. 2009; 70:390–395.
29. Lukić MJ, Veselinović Lj, Stojanović Z, Maček-Kržmanc M, Bračko I, Škapin SD, Marković S, Uskoković D. Peculiarities in sintering behavior of Ca-deficient hydroxyapatite nanopowders. Mat Lett. 2012; 68:331–335.
30. Hodge HC, LeFevre ML, Bale WF. Chemical and X-Ray Diffraction Studies of Calcium Phosphates. Indust Eng Chem Anal Ed. 1938; 10:156–161.
31. Sadat-Shojai M, Khorasani MT, Jamshidi A. Chemical Precipitation of Hydroxyapatite Nanoparticles – A Taguchi Experimental Design Approach. Mat Chem Phys. 2012 in press.
32. Kibalczyc W, Zielenkiewicz A, Zielenkiewicz W. Calorimetric investigations of calcium phosphate precipitation in relation to solution composition and temperature. Thermochim Acta. 1988; 131:47–55.
33. Mahapatra PP, Mishra H, Chickerur NS. Solubility of Hydroxyapatite and Related Thermodynamic Data. Thermochim Acta. 1982; 52:333–336.
34. Lin FH, Liao CJ, Chen KS, Sun JS, Liu HC. Degradation behaviour of a new bioceramic: $Ca_2P_2O_7$ with addition of $Na_4P_2O_7 \cdot 10H_2O$. Biomat. 1997; 18:915–921.
35. Narasaraju TSB, Phebe DE. Some physico-chemical aspects of hydroxylapatite. J Mat Sci. 1996; 31:1–21.
36. Pan HB, Darvell BW. Calcium Phosphate Solubility. Crys Grow Des. 2009; 9:639–645.
37. Levinskas GJ, Neuman WF. The Solubility of Bone Mineral. J Phys Chem. 59:164–168. 195.
38. Kirkham J, Firth A, Vernals D, Boden N, Robinson C, Shore RC, Brookes SJ, Aggeli A. Physico-chemical properties of crystal surfaces in matrix–mineral interactions during mammalian biomineralisation. Curr Opin Coll Interface Sci. 2002; 7:124–132.
39. Hole BB, Keller DS, Burry WM, Schwarz JA. Surface energetics of bone mineral and synthetic hydroxyapatite using inverse gas chromatography. J Chromatography B. 2011; 879:1847–1850.

40. Santos EA, Farina M, Soares GA, Anselme K. Surface energy of hydroxyapatite and β-TCP ceramics driving serum protein adsorption and osteoblast adhesion. J Mat Sci Mat Med. 2007; 19:2307–2316.

41. Engel E, Del Valle S, Aparicio C, Altankov G, Asin L, Planell JA, Ginebra MP. Discerning the Role of Topography and Ion Exchange in Cell Response of Bioactive Tissue Engineering Scaffolds. Tissue Eng A. 2008; 14:1341–1351.

42. Boyan BD, Lossdörfer S, Wang L, Zhao G, Lohmann CH, Cochran DL, Schwartz Z. Osteoblasts generate an osteogenic microenvironment on surfaces with rough microtopographies. Eur Cell Mater. 2003; 6:22–27. [PubMed: 14577052]

43. Wang Y, Zhang S, Zeng X, Cheng K, Qian M, Weng W. In vitro behavior of fluoridated hydroxyapatite coatings in organic-containing simulated body fluid. Mat Sci Eng C. 2007; 27:244–250.

44. Mavropoulos E, Costa AM, Costa LT, Achete CA, Mello A, Granjeiro JM, Rossi AM. Adsorption and bioactivity studies of albumin onto hydroxyapatite surface. Coll Surf B: Biointerfaces. 2011; 83:1–9.

45. Mazin AL. Hydroxyapatite Thin-Layer Chromatography of Nucleic Acid. Mol Bio. 1977; 11:477–498.

46. Fargues PC, Bailly M, Grevillot G. Adsorption of BSA and Hemoglobin on Hydroxyapatite Support: Equilibria and Multicomponent Dynamic Adsorption. Adsorption – J Int Adsorp Soc. 1998; 4:5–16.

47. Besarab A, DeGuzman A, Swanson JW. Effect of albumin and free calcium concentrations on calcium binding in vitro. J Clin Pathol. 1981; 34:1361–1367. [PubMed: 7328183]

48. Mueller B, Zacharias M, Rezwan K. Bovine Serum Albumin and Lysozyme Adsorption on Calcium Phosphate Particles. Adv Eng Mater. 2010; 12:B53–B61.

49. Leonhardt H, Gordon L, Livingston R. Acid-base equilibriums of fluorescein and 2',7'-dichlorofluorescein in their ground and fluorescent states. J Phys Chem. 1971; 75:245–249.

50. Bernards DA, Desai TA. Nanotemplating of Biodegradable Polymer Membranes for Constant-Rate Drug Delivery. Adv Mater. 2010; 22:2358–2362. [PubMed: 20376851]

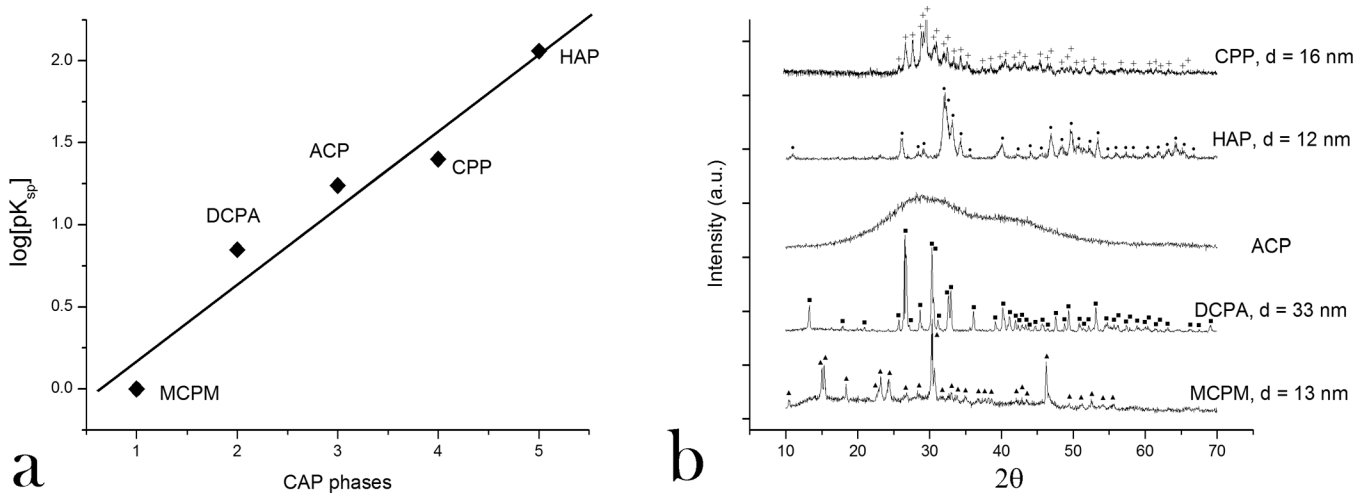

Fig.1.

(a) A double logarithmic curve showing literature-derived solubility products (K_{sp}) for different CAP phases synthesized; (b) X-ray diffractograms of five different monophasic CAP powders prepared: MCPM, DCPA, ACP, HAP, and CPP. Crystallographic planes corresponding to the given phases are labeled with the following symbols: MCPM - ▲; DCPA – ■; HAP - ●; CPP - +.

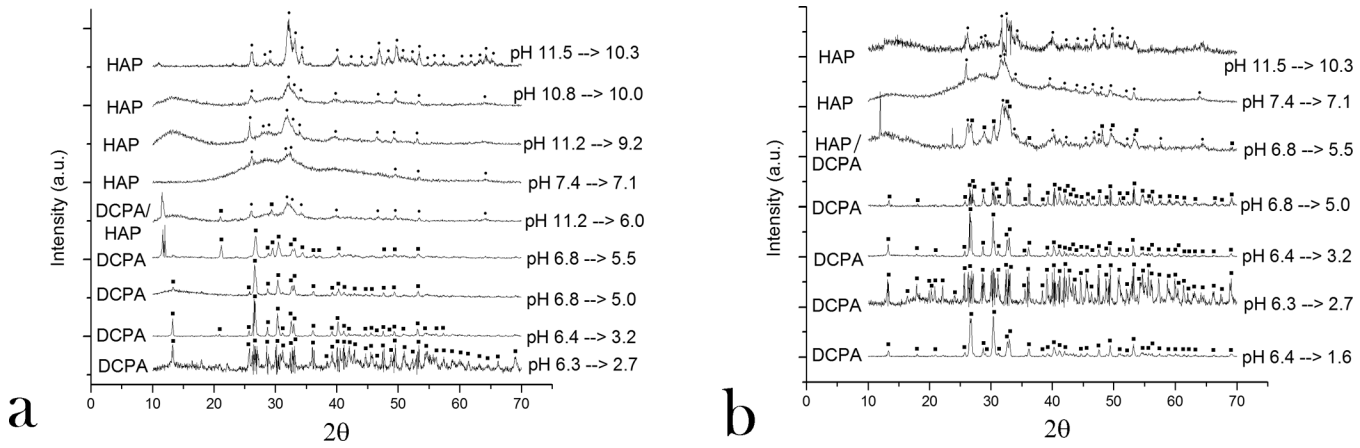

Fig.2.

X-ray diffractograms of CAP powders synthesized by means of the precipitation method used to prepare HAP at different pHs of the initial $Ca(NO_3)_2$ solution (x→) and of the solution in equilibrium with the precipitate (→x), without (a) and with (b) the boiling step following mixing of the reactants. Crystallographic planes corresponding to HAP and DCPA are labeled with the following symbols: DCPA – ■; HAP - ●.

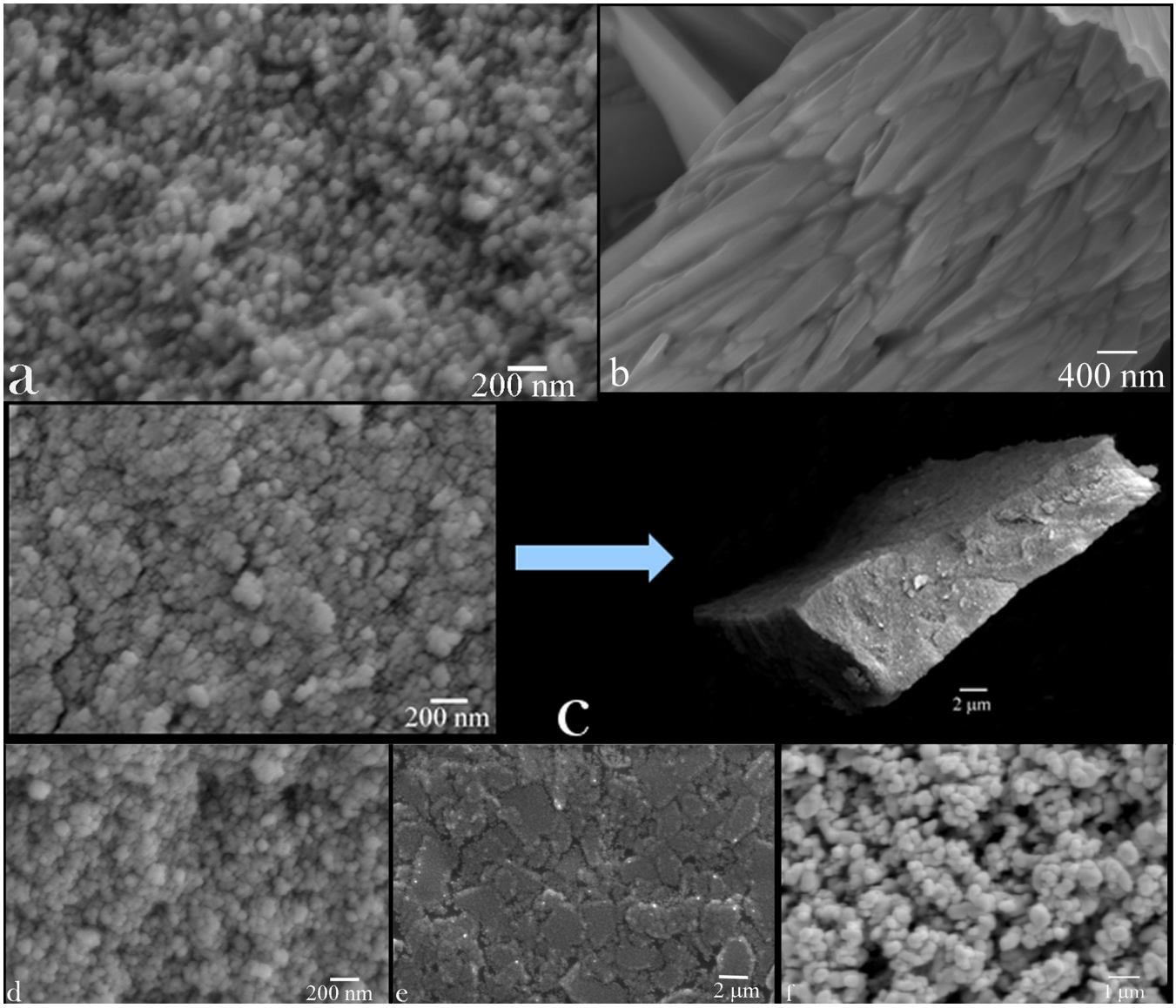

Fig.3.

(a, b) SEM images of DCPA powder prepared with (a) and without (b) the boiling treatment as a synthesis step; (c) nanosized spherical particles of HAP acting as subunits in microscopic blocks of material formed by aggregation during desiccation of the powder; SEM images showing spherical morphologies of monophasic and nanosized CAP powders other than HAP and DCPA: (d) ACP; (e) MCPM; (f) CPP.

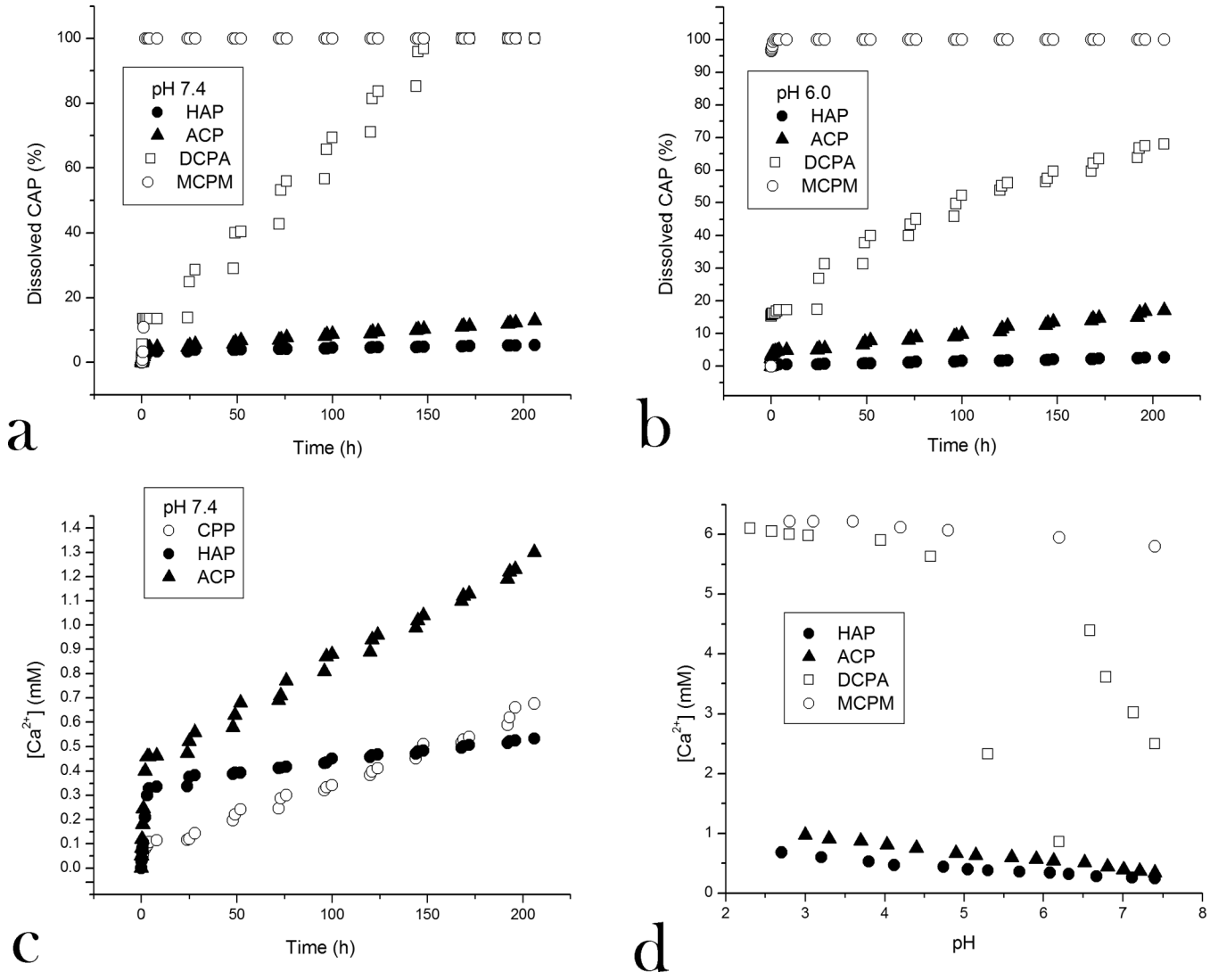

Fig.4.

Percentage of the dissolved CAP as a function of the incubation time at pHs 7.4 (a) and 6.0 (b); (c) cumulative increase in the concentration of calcium ions in the supernatant over time, directly indicative of solubility of the compound, for CPP, ACP and HAP; and (d) concentration of free Ca^{2+} ions, directly indicative of the compound's solubility, as a function of pH in solutions over different solid CAP phases.

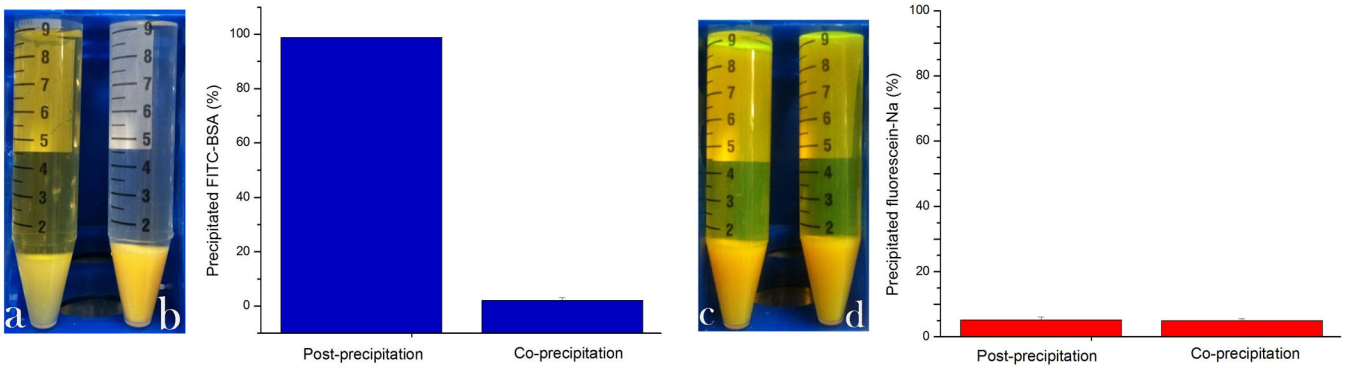

Fig.5.

Visual appearance of HAP powders loaded with BSA (a, b) and fluorescein (c, d) using the co-precipitation (a, c) and post-precipitation method (b, d), along with the respective loading efficiencies.

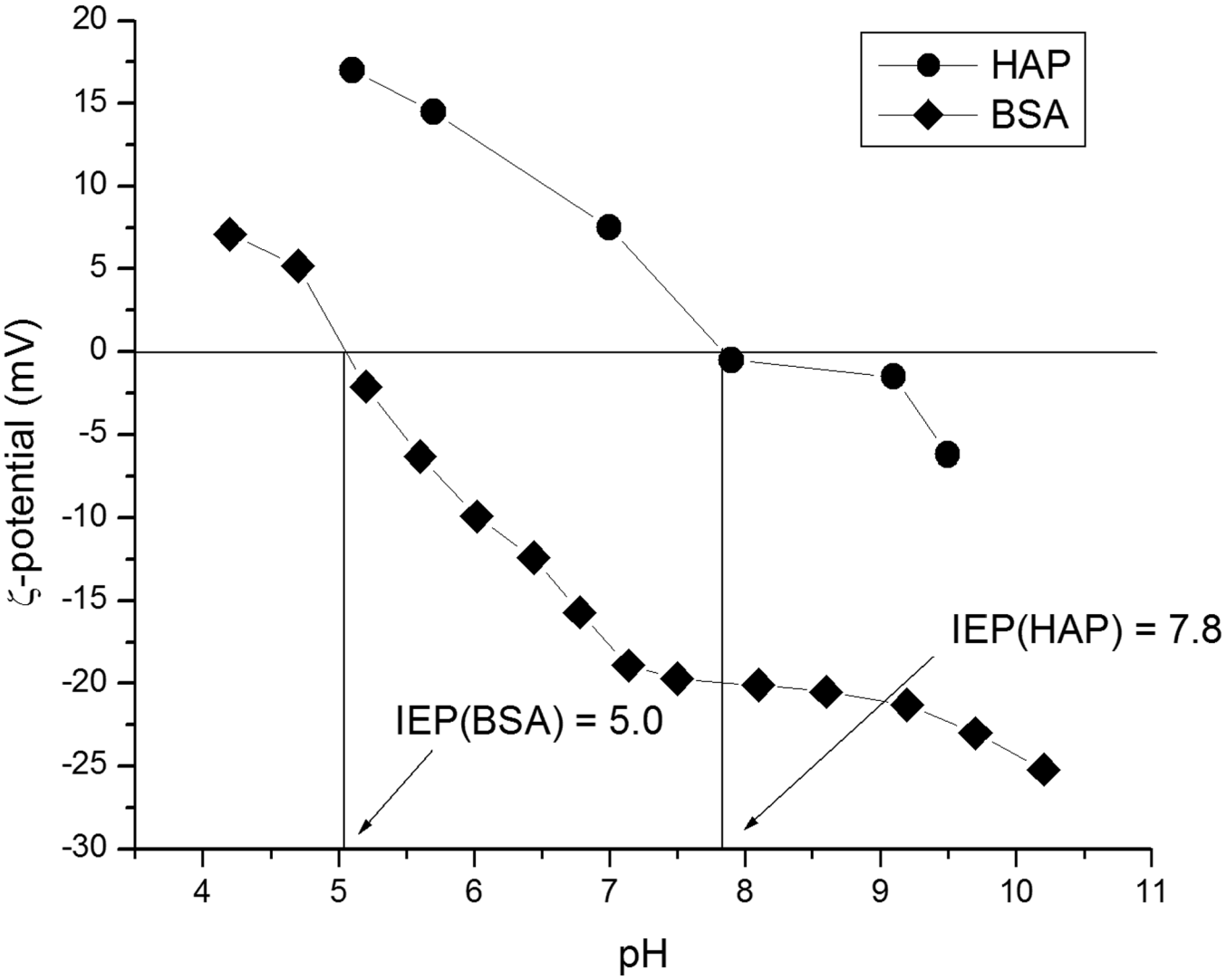

Fig.6.
Zeta potential vs. pH curves for BSA and fresh HAP precipitates from aqueous solution, denoting isoelectric points (IEP) determined for both.

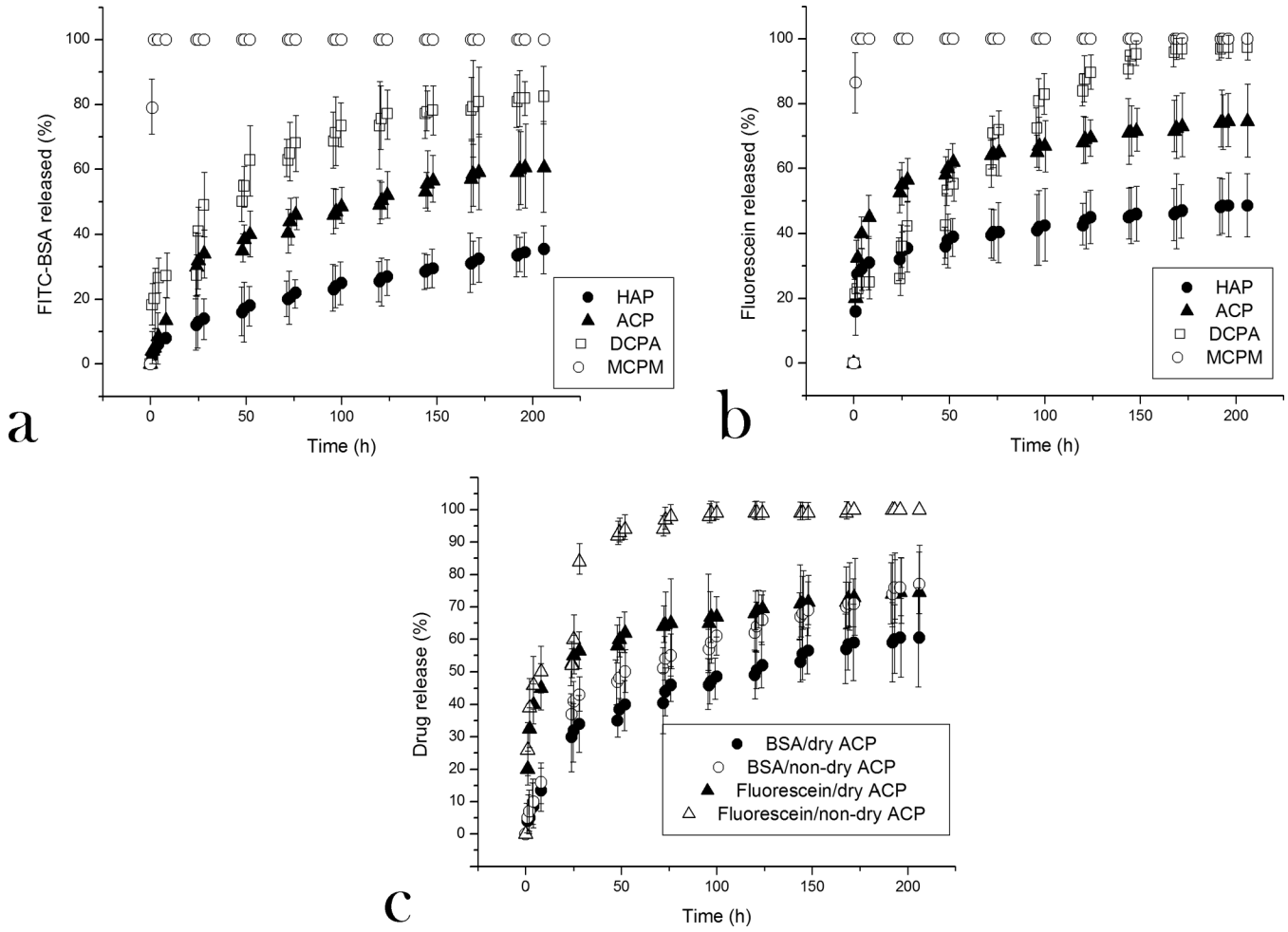

Fig.7.

Time release profiles for BSA (a) and fluorescein (b) encapsulated within CAP powders of different phase composition, and a comparison between time release profiles for BSA and fluorescein molecules encapsulated within dried/agglomerated and undried/non-agglomerated ACP powders (c). Data points are given as averages with error bars representing the standard deviation.

Table 1

Main CAP phases.[13–16]

Phase	Chemical formula	Space group	pK_{sp} at 37 °C	Ca/P molar ratio
MCPA *	$Ca(H_2PO_4)_2$	Triclinic $P\bar{1}$	1.14	0.5
MCPM *	$Ca(H_2PO_4)_2{\cdot}H_2O$	Triclinic $P\bar{1}$	1.14	0.5
DCPD *	$CaHPO_4{\cdot}2H_2O$	Monoclinic I_a	6.6	1
DCPA *	$CaHPO_4$	Triclinic $P\bar{1}$	7.0	1
β-CPP *	$Ca_2P_2O_7$	Tetragonal $P4_1$	18.5	1
ACP *	$Ca_3(PO_4)_2{\cdot}nH_2O$	/	25	1.3–1.5
α-TCP *	$Ca_3(PO_4)_2$	Monoclinic $P2_1/a$	25.5	1.5
β-TCP *	$Ca_3(PO_4)_2$	Rhombohedral R3cH	29.5	1.5
TTCP *	$Ca_4(PO_4)_2O$	Monoclinic $P2_1$	37.5	2
OCP *	$Ca_8H_2(PO_4)_6{\cdot}5H_2O$	Triclinic $P\bar{1}$	97.4	1.33
HAP *	$Ca_{10}(PO_4)_6(OH)_2$	Pseudo-Hexagonal $P6_3/m$	117.3	1.67

* MCPA = monocalcium phosphate anhydrous; MCPM = monocalcium phosphate monohydrate; DCPD = dicalcium phosphate dehydrate; DCPA = dicalcium phosphate anhydrous; CPP = calcium pyrophosphate; ACP = amorphous calcium phosphate (data pertain to the phase obtainable at pH 9 – 11); TCP = tricalcium phosphate; TTCP = tetracalcium phosphate; OCP = octacalcium phosphate; HAP = hydroxyapatite.

Table 2

Initial ionic concentrations during the synthesis of CAP powders of different monophase compositions by precipitation at different pHs and temperatures.

Phase	$[Ca^{2+}]$ (M)	pH of $Ca^{2+}_{(aq)}$	$[H_xPO_4^{3-x}]$ (M)	pH of $H_xPO_4^{3-x}_{(aq)}$	Final pH	Boiling	d (nm)
HAP	0.1	11.5	0.06	10.5	10.3	Yes	12
HAP	0.1	11.5	0.06	10.5	10.3	No	18
ACP	0.5	6.8	0.2	10.5	10.0	No	/
β-CPP*	0.2	11.2	0.15	6.8	6.0	No	16
DCPA	0.33	6.8	0.25	7.6	5.0	Yes	59
DCPA	0.33	6.8	0.25	7.6	5.0	No	33
MCPM	1.8	6.2	3.5	0.25	0.1	No	3

*CPP was prepared by thermal annealing at 800 °C in air for 2 h following precipitation.

Table 3

Dissolution time scales and rates for four different CAP powders: HAP, ACP, DCPA and MCPM at two different pHs: 7.4 and 6.0.

Phase	pH	$[Ca^{2+}]_{total}$	Dissolution rate ($[Ca^{2+}]$/day) (mM)	Dissolution rate (%CAP/day)	Time to complete dissolution*	Time to complete dissolution**
HAP	7.4	10	0.025	0.25	≈ 1 year	≈ 2 months
ACP	7.4	10	0.1	1	≈ 3 months	≈ 1 week
DCPA	7.4	5.8	0.84	14.5	≈ 1 week	≈ 10 h
MCPM	7.4	3.7	3.7	100	≈ 1–2 h	≈ 1–2 h
HAP	6.0	10	0.03	0.3	≈ 1 year	≈ 2 months
ACP	6.0	10	0.15	1.5	≈ 2 months	≈ 2 weeks
DCPA	6.0	5.8	0.3	5.2	≈ 2–3 weeks	≈ 3 days
MCPM	6.0	3.7	3.7	100	≈ 1–2 h	≈ 1–2 h

*24 h medium replacement

**Extrapolation of 1 h medium replacement